# Solution Structure of Human SUMO-3 C47S and Its Binding Surface for Ubc9[†,‡]

Husheng Ding, Yingqi Xu, Quan Chen, Haiming Dai, Yajun Tang, Jihui Wu,* and Yunyu Shi*

*School of Life Sciences, University of Science and Technology of China, and Hefei National Laboratory for Physical Sciences at Microscale, Hefei, Anhui 230026, People's Republic of China*

*Received October 20, 2004; Revised Manuscript Received December 10, 2004*

ABSTRACT: Small ubiquitin-related modifier SUMO-3 is a member of a growing family of ubiquitin-like proteins (Ubls). So far, four isoforms of SUMO have been identified in humans. It is generally known that SUMO modification regulates protein localization and activity. Previous structure and function studies have been mainly focused on SUMO-1. The sequence of SUMO-3 is 46% identical with that of SUMO-1; nevertheless, functional heterogeneity has been found between the two homologues. Here we report the solution structure of SUMO-3 C47S (residues 14−92) featuring the $\beta$-$\beta$-α-$\beta$-$\beta$-α-$\beta$ ubiquitin fold. Structural comparison shows that SUMO-3 C47S resembles ubiquitin more than SUMO-1. On the helix−sheet interface, a strong hydrophobic interaction contributes to formation of the globular and compact fold. A Gly-Gly motif at the C-terminal tail, extending away from the core structure, is accessible to enzymes and substrates. In vivo, SUMO modification proceeds via a multistep pathway, and Ubc9 plays an indispensable role as the SUMO conjugating enzyme (E2) in this process. To develop a better understanding of SUMO-3 conjugation, the Ubc9 binding surface on SUMO-3 C47S has been detected by chemical shift perturbation using NMR spectroscopy. The binding site mainly resides on the hydrophilic side of the $\beta$-sheet. Negatively charged and hydrophobic residues of this region are highly or moderately conserved among SUMO family members. Notably, the negatively charged surface of SUMO-3 C47S is highly complementary in its electrostatic potentials and hydrophobicity to the positively charged surface of Ubc9. This work indicates dissimilarities between SUMO-3 and SUMO-1 in tertiary structure and provides insight into the specific interactions of SUMO-3 with its modifying enzyme.

Protein sumoylation by small ubiquitin-related modifier (SUMO) proteins is an important posttranslational regulatory modification in diverse cellular processes, including nuclear transport, gene expression, stress responses, cell cycle control, oncogenesis, and response to virus infection (*1*, *2*). It has been proposed that SUMO conjugation may function antagonistically with respect to ubiquitin conjugation and/or that SUMO conjugation may regulate the interaction of the target protein with other cellular components. In humans, four types of SUMOs, i.e., SUMO-1−4, have been identified (*3*, *4*). All SUMO genes actually encode an inactive precursor bearing a short C-terminal peptide, which is cleaved off by SUMO-specific proteases (SENPs) to produce the mature Gly-Gly C-terminus. The SUMO molecule is then adenylated and covalently linked to a SUMO-activating E1 enzyme. Subsequently, SUMO is transferred to the SUMO-conjugating E2 enzyme, Ubc9. Then the E3 ligases stimulate conjugation of SUMO to specific substrates through an isopeptide bond formed between the C-terminal glycine residue of SUMO and a lysine residue in the substrate (*5*). This lysine is frequently found at a conserved ΨKXE motif, where Ψ is a hydrophobic amino acid residue and X is any residue (*6*). Importantly, sumoylation is a dynamic and reversible process. Genetic data from yeast have shown that SUMO deconjugation catalyzed by Ulp1 (a SUMO-specific protease) is required for cell cycle progression (*7*).

Sequence alignment of SUMO-1−3 reveals that the sequences of SUMO-2 and -3 are 46−48% identical with that of SUMO-1 while SUMO-2 and -3 are closely related and are 97% identical in sequence, and it is reasonable to group SUMO-2 and -3 into a subfamily distinct from SUMO-1. SUMO-4, associated with the pathogenesis of type I diabetes, is 87% homologous with SUMO-2 with respect to amino acid sequence (*4*). Some substrates can be modified equally well by SUMO-1 and SUMO-2/3; however, Ran GTPase activating protein 1 (RanGAP1) is predominantly modified by SUMO-1, and topoisomerase II is preferentially modified by SUMO-2/3 (*8*−*10*). It is likely that E3s mediate the differential conjugation of the SUMO isoforms. To date, the mechanisms that determine selective modification by specific SUMO isoforms are not known. In COS-7 cells, conjugation of SUMO-2/3 is strongly induced in response to various stresses but SUMO-1 conjugation is not; thus, one function of SUMO-2/3 may be to provide a reservoir of free SUMO for stress responses (*8*). Unlike SUMO-1, SUMO-2−4 contain a ΨKXE motif in their N-terminal extensions, which can serve as SUMO attachment sites, thereby allowing

[†] This work was supported by the Chinese National Fundamental Research Project (Grants G1999075605 and 2002CB713806), the Chinese National Natural Science Foundation (Grants 30270293 and 30121001), the Key Project of the National High Technology Research and Development Program of China (Grant 2002BA711A13), and the Pilot Project of the Knowledge Innovation Program of the Chinese Academy of Science (Grant KSCX1-SW-17).

[‡] The atomic coordinates have been deposited in the Protein Data Bank as entry 1U4A.

* To whom correspondence should be addressed. Telephone: 86-551-3607464. Fax: 86-551-3601443. E-mail: wujihui@ustc.edu.cn or yyshi@ustc.edu.cn.

10.1021/bi0477586 CCC: $30.25 
Published on Web 02/04/2005

formation of poly-SUMO chains (*11*). This may be one of the molecular foundations for functional heterogeneity between SUMO-1 and SUMO-2/3.

Human Ubc9, composed of 158 amino acid residues, belongs to an E2 protein family. In contrast to multiple E2 enzymes identified in ubiquitylation, Ubc9 is the only known SUMO-conjugating E2 enzyme. The crystal structure of human Ubc9 has been determined, and it possesses a considerably stronger electrostatic dipole (*12*). The three-dimensional structure of human SUMO-1 was determined using homonuclear NMR[1] and heteronuclear NMR. Though only 18% identical in sequence with ubiquitin, the overall structure is similar to that of ubiquitin (*13*−*16*). Despite the similar protein fold, the distribution of charged residues on the surface of SUMO-1 is very different from that of ubiquitin. The binding interfaces of the Ubc9 and SUMO-1 complex have been detected by chemical shift perturbation. It was shown that the binding site of SUMO-1 resides on the ubiquitin domain, and the binding site of Ubc9 is located on a structurally conserved region of E2 (*17*). Smt3 is the SUMO homologue in yeast. Its NMR structure and the crystal structure of the Smt3−Ulp1 complex have also been determined (*18*, *19*). The structural comparison of Smt3 in free and Ulp1 complex forms indicates important structural changes of Smt3 in complex as a result of the protein−protein interaction.

Most previous studies have been focused on SUMO-1; now more attention shifts to other SUMO family members. In this paper, we report the solution structure of SUMO-3 C47S and study its binding to Ubc9 by chemical shift perturbation using NMR spectroscopy. This work indicates structure dissimilarities of SUMO-3 with its homologue, SUMO-1, and provides insight into the specific interactions of SUMO-3 C47S with its modifying enzyme, Ubc9.

## MATERIALS AND METHODS

*Choice of Sequence for the NMR Study.* The full-length cDNA of SUMO-3 (103 amino acid residues) was cloned and expressed initially; however, unfortunately, the signal-to-noise ratio of peaks in the $^{1}H-^{15}N$ HSQC spectrum was seriously uneven, and the quality of CBCANH and CBCA(CO)NH spectra was not sufficiently good to complete the backbone assignment. Thus, we analyzed its secondary structures using various algorithms and sequence alignment, and less ordered structures were identified in both N- and C-terminal regions of SUMO-3. As is generally known, flexible terminal regions prove to be difficult to resolve in solution NMR analyses. On the basis of these predictions and the previous study, residues 14−92, a ubiqutin-like domain of SUMO-3, were chosen for the NMR study. In addition, the C47S mutation of SUMO-3 was introduced to prevent the molecular dimerization by removal of the intermolecular S−S bridge.

*Cloning, Expression, and Purification of SUMO-3 C47S.* The DNA fragment encoding residues 14−92 of SUMO-3 was amplified from the human brain cDNA library (Clontech) by a polymerase chain reaction (PCR) using the two primers 5′-CTCGAGACCTCCCGTCTGCTGCTGGAAC-3′ and 5′-CATATGAATGACCACATCAACCTG-3′ (Sangon) designed on the basis of the mRNA sequence of human SUMO-3 (GenBank accession number BC000036); these oligonucleotides were introduced with *Nde*I and *Xho*I restriction sites, respectively. The reaction product (∼250 bp) was purified and then cloned into the T-vector. The positive clones were identified by restriction digestion. Then the DNA fragment was ligated into the *Nde*I−*Xho*I-cleaved plasmid pET22b (Novagen). The recombinant vector was amplified in *Escherichia coli* BL21(DE3). Subsequently, the plasmid-inserted SUMO-3 DNA fragment (encoding residues 14−92) was extracted and used as the template for site-directed mutagenesis for C47S (TGC → AGC). Two internal primers, 5′-CTGATGAAGGCCTACAGCGAGAGGCAGGGCTTG-TC-3′ and 5′-GACAAGCCCTGCCTCTCGCTGTAGGC-CTTCATCAG-3′ (Sangon), were designed for it. The mutation of the gene was confirmed by DNA sequencing (Takara). Taq polymerase, Ex Taq polymerase, T-vector, DNA ligase, and the relevant restriction enzymes were obtained from Takara. The mutated plasmid was then transformed into *E. coli* BL21(DE3) for expression. Recombinant SUMO-3 C47S has 88 amino acid residues, including a C-terminal His tag (LEHHHHHH). Uniformly labeled recombinant SUMO-3 C47S was produced using minimal medium containing 0.5 g/L [$^{15}N$]ammonium sulfate (99%) and 2.5 g/L [$^{13}C$]glucose (99%) as the sole nitrogen and carbon sources, respectively. SUMO-3 C47S was purified using a Ni-chelating column (Qiagen) and then Sephadex G-50 gel filtration (Pharmacia).

*Expression and Purification of Ubc9.* The expression plasmid (pGEX-Ubc9) was transformed into *E. coli* DH5α cells. Expression was induced once the optical absorption at 600 nm ($A_{600}$) reached 0.7 via addition of 0.8 mM IPTG for 6 h. Cells were lysed with a sonifier, and a 100000*g* supernatant was used for protein purification. The fusion protein was purified on a GSH−Sepharose 4B column (Pharmacia) according to the manufacturer's specification. The GST−Ubc9 fusion protein was digested with 50 units/mL thrombin and then purified on a Sephadex G-50 column (Pharmacia).

*Purity Identification and Concentration Measurement.* The purities of SUMO-3 C47S and Ubc9 were confirmed by SDS−PAGE, and the concentrations were measured with BCA kits (Pierce). The concentrations of $^{15}N$-labeled and $^{13}C$- and $^{15}N$-labeled SUMO-3 C47S were ∼0.6−0.8 mM, while the concentration of unlabeled Ubc9 was up to 1.3 mM. All the samples for NMR contained 25 mM phosphate buffer (pH 6.25), 75 mM NaCl, and 1 mM EDTA in a 90% $H_2O$/10% $D_2O$ mixture.

*NMR Spectroscopy and Data Processing.* The NMR experiments were performed on a Bruker DMX500 spectrometer with self-shielded *z*-axis gradients. The following spectra were recorded at 298 K to obtain backbone and side chain resonance assignments: 2D $^{1}H-^{15}N$ HSQC (*20*), 2D $^{1}H-^{13}C$ HSQC (*20*), 3D triple-resonance spectra HNCO (*21*), HN(CA)CO (*22*), CBCA(CO)NH (*23*), CBCANH (*24*), C(CO)NH-TOCSY (*25*), H(CCO)NH-TOCSY (*25*), $^{15}N$ TOCSY, HCCH-TOCSY (*26*), HCCH-COSY (*27*), HBHA(CBCACO)NH (*28*), and 2D CB(CC)HD-COSY (aromatics) (*29*). 3D $^{15}N$-separated and $^{13}C$-separated NOESY (*30*) were

[1] Abbreviations: NMR, nuclear magnetic resonance; 2D and 3D, two- and three-dimensional, respectively; HSQC, heteronuclear single-quantum correlation; NOE, nuclear Overhauser effect; NOESY, nuclear Overhauser effect spectroscopy; TOCSY, total correlated spectroscopy; rmsd, root-mean-square deviation.

acquired with mixing time of 100 and 130 ms, respectively.

The $^{15}$N-labeled sample was lyophilized and dissolved in 99.96% $D_2O$ which was followed immediately with HSQC experiments for monitoring the disappearance of NH signals at 292 K. After all of the peaks had vanished, 2D homonuclear TOCSY and NOESY spectra were recorded on this sample at 298 K, which exhibited proton resonance from aromatic rings exclusively in the region beyond 6.0 ppm.

NMR data processing was carried out using NMRPipe and NMRDraw software, and the data were analyzed with PIPP. All software was run on a Linux system. Linear prediction (*31*) was used to improve the spectral resolution in the indirect dimensions where constant-time acquisition was used, for example, the $^{15}$N evolution dimension in all the triple-resonance experiments mentioned above.

*Experimental Restraints and NMR Structure Calculation.* NMR distance restraints were collected from three different NOESY spectra: 3D $^{15}$N-separated NOESY in water for amide protons, 3D $^{13}$C-separated NOESY in water for aliphatic protons, and 2D $^1$H NOESY in $D_2O$ (mixing time of 100 ms) for aromatic protons. NOE restraints were grouped into four distance ranges: strong, 1.8−3.0 and 1.8−3.5 Å; medium, 1.8−4.0 and 1.8−4.5 Å; weak, 1.8−5.0 Å; and very weak, 1.8−6.0 Å. Considering that the spin diffusion effect could be serious for aliphatic and aromatic protons, a more conservative distance estimation was used for the latter two NOESY spectra; therefore, most medium-range and long-range NOEs from these two spectra were put into the weak or very weak groups, while most intraresidue NOEs were not used. The 1.8 Å lower limits were imposed only implicitly by the van der Waals repulsion force. For methyl protons, non-stereospecifically assigned methylene protons, and aromatic ring protons, $r^{-6}$ summation averages were applied (*32*).

The chemical shift index (CSI) (*33*) was calculated for four types of nuclei: Cα, C$\beta$, C′, and Hα. The derived secondary structures based on the consensus CSI were converted into restraints on $\varphi$ and $\psi$ angles. For α-helix residues, $\varphi$ was limited to $-60 \pm 40°$ while $\psi$ was limited to $-50 \pm 50°$; for $\beta$-strand residues, $\varphi$ was limited to $-120 \pm 40°$ while $\psi$ was limited to $130 \pm 50°$. Hydrogen bond restraints were employed in areas of regular secondary structures, displaying characteristic NOE cross-peaks. Each deduced hydrogen bond was represented by two distance constraints: α-helix residues, 1.6−2.4 Å for $H^N\cdots O$ bonds and 2.4−3.3 Å for N···O bonds; and $\beta$-strand residues, 1.4−2.7 Å for $H^N\cdots O$ bonds and 2.4−3.7 Å for N···O bonds.

Structures were calculated using CNS version 1.1 (*34*), employing a simulated annealing protocol for torsion angle dynamics (*35*). For the initial rounds of structure calculations, only sequential, intraresidual, medium-range NOEs, unambiguous long-range NOEs, and dihedral angle restraints were used. Later, all other long-range NOEs and hydrogen bonds were introduced in consecutive steps. Simple impulsion nonbonded interactions were used during structure calculation.

*Chemical Shift Perturbation.* To detect the Ubc9 binding site on SUMO-3 C47S, 0.4 mM $^{15}$N-labeled SUMO-3 C47S was used. After the $^1$H−$^{15}$N HSQC spectrum of free SUMO-3 C47S was recorded, the sample was titrated with 1.3 mM unlabeled Ubc9. The final concentrations of both proteins at the end of the titration were approximately 0.3 mM. The HSQC spectra for obtaining the Ubc9 binding surface on SUMO-3 C47S were recorded at 298 K, which was used for the resonance assignments of SUMO-3 C47S.

## RESULTS AND DISCUSSION

*Resonance Assignment.* The 2D $^1$H−$^{15}$N HSQC spectrum of SUMO-3 C47S illustrates good dispersion of the proton and nitrogen resonances in the amide groups. In this spectrum, 77 expected correlation peaks for the backbone amide resonances were assigned, excluding N14 (N14 is the second residue of the truncated protein, and its residue number is the same as that in SUMO-3). The backbone assignments of SUMO-3 C47S were made primarily on the basis of CBCANH and CBCA(CO)NH spectra, with the use of HNCO and HN(CA)CO spectra to resolve ambiguities. C(CO)NH TOCSY and H(CCO)NH TOCSY were used to obtain side chain $^{13}$C and $^1$H chemical shifts, respectively. HCCH-TOCSY and HCCH-COSY were then used to resolve the ambiguities inside side chains; some side chain resonances missed in C(CO)NH or H(CCO)NH were also found and assigned. The water peak did not interfere with these two spectra seriously since most Hα chemical shifts were $<4.50$ or $>4.90$ ppm. Some aromatic ring proton chemical shifts were assigned by correlating H$\delta$ to C$\beta$ in CB(CC)-HD-COSY spectra, as well as 2D TOCSY spectra in $D_2O$; the others were assigned through NOEs between ring protons and the intraresidue H$\beta$ and HN atoms. In total, ∼95% of the side chain resonances were assigned.

*Secondary Structures.* Figure 1 shows the NOE pattern of short- and medium-range NOEs defining the secondary structure. The region from L39 to Q50 shows NOE patterns typical for an α-helical conformation. Six slowly exchanging NH protons (M43, A45, Y46, S47, E48, and R49) were found within this region, indicating that protection occurs most likely due to formation of hydrogen bonds here. In addition, a few helix-typical NOEs were found in the region from P72 to E76. Two slowly exchanging NH protons (L75 and E76) further indicate the second α-helix at this position. In contrast, helix α2 is not completely detected when the CSI method is applied.

Characteristic long-range backbone NOE connectivities ($i - j > 4$) were used to define $\beta$-strands. On the basis of this standard, five $\beta$-strands [residues 17−23 ($\beta$1), 27−33 ($\beta$2), 58−61 ($\beta$3), 64−66 ($\beta$4), and 80−86 ($\beta$5)] were identified with $\beta$1 and $\beta$2, $\beta$3 and $\beta$4, and $\beta$3 and $\beta$5 being antiparallel and $\beta$1 and $\beta$5 being parallel. These secondary structural elements were additionally traced by 18 slowly exchanging NH protons. Some isolated $d\alpha_N(i, i + 2)$ and/or $d_{NN}(i, i + 2)$ NOE contacts indicate the presence of $\beta$-turns (residues 23−26, 34−37, 53−56, and 61−64). The location and extent of the secondary structural elements were further confirmed by CSI. Generally speaking, the secondary structural elements identified by this approach are mainly in agreement with those found by NOEs. A CSI plot for the resonances of SUMO-3 C47S is also shown in Figure 1.

*Quality of the SUMO-3 C47S Structure.* The SUMO-3 C47S structure was calculated using CNS version 1.1 (*34*). A total of 1406 interproton restraints, including 360 intraresidue, 395 sequential, 225 medium-range, and 426 long-range, together with 78 backbone dihedral angle constraints and 28 hydrogen bond constraints were used in the final

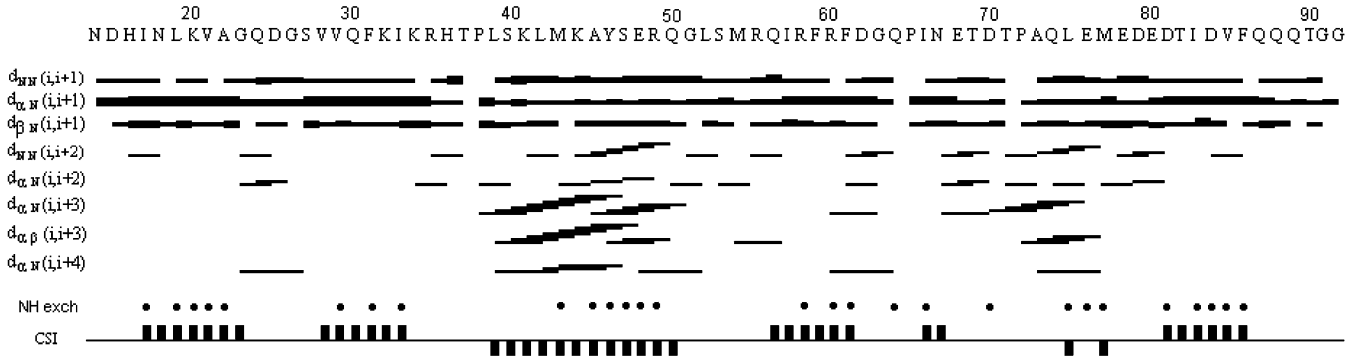


FIGURE 1: Summary of sequential and medium-range NOE patterns observed in SUMO-3 C47S. The data are derived from $^{15}$N-separated NOESY and $^{13}$C-separated NOESY spectra. The thickness of the bars of sequential NOEs indicates the relative intensities of the corresponding cross-peaks in NOESY, and horizontal lines indicate the observation of medium-range NOEs between residue pairs. Filled circles denote the locations of slowly exchanging amide protons. The short bars at the bottom represent consensus CSI predictions from Cα, C$\beta$, C′, and Hα chemical shifts; bars below the line mean an index of −1, while those above the line mean an index of +1. Four or more consecutive bars with values of −1 not interrupted by a bar with a value of +1 indicate α-helix. Three or more consecutive bars with values of +1 not interrupted by a bar with a value of −1 indicate $\beta$-strand.

Table 1: NMR Structure Statistics for SUMO-3 C47S

| | |
|---|---|
| (a) NMR restraints | |
| distance restraints | 1406 |
| intraresidue | 360 |
| sequential ($\|i-j\|=1$) | 395 |
| medium-range ($\|i-j\|<5$) | 225 |
| long-range ($\|i-j\|\geq 5$) | 426 |
| dihedral angle restraints | 78 |
| hydrogen bonds | 28 |
| (b) statistics for 20 SA structures | |
| rmsd from idealized covalent geometry | |
| bonds (Å) | $0.0008 \pm 0.00004$ |
| angles (deg) | $0.2819 \pm 0.0023$ |
| impropers (deg) | $0.1022 \pm 0.0040$ |
| Lennard-Jones potential energy (kcal/mol) | $-221.68 \pm 13.97$ |
| (c) coordinate precision | |
| pairwise rmsd for backbone atoms (residues 17−86) (Å) | $0.79 \pm 0.11$ |
| pairwise rmsd for heavy atoms (residues 17−86) (Å) | $1.62 \pm 0.14$ |
| rmsd from the mean | |
| residues 17−86 (Å) | 0.54/1.11[a] |
| residues 17−23, 27−33, 39−50, 58−61, 64−66, 72−76, 80−86 (Å) | 0.46/0.97[a] |
| (d) Ramachandran plot (%) | |
| residues in most favored regions | 74.3 |
| residues in additional allowed regions | 24.4 |
| residues in generously allowed regions | 1.0 |
| residues in disallowed regions | 0.2 |

[a] Backbone atoms/heavy atoms.

round of the structural calculation. Being unassigned, the first residue (M13) and the C-terminal His tag had no NMR restraints, and they were excluded from structure calculation. Thus, on average, every amino acid residue is characterized by 18 contacts with its neighbors. Distributions of restraints by range and by sequence position are shown in Table 1 and Figure 2A, respectively. At the final stage, 200 conformers were calculated; of these, 20 conformers with the lowest energy were selected. All of them have no distance violations larger than 0.5 Å and no angle violations of more than 5°. In the 20 selected structures, 74.3% of the residues were in the most favored region on the Ramachandran plot using PROCHECK (*36*), 24.4% in the additionally allowed region, 1.0% in the generously allowed region, and 0.2% in the disallowed region.

For the well-defined region of SUMO-3 C47S (residues 17−86), the values of the rmsd from the mean structure were 0.54 Å for backbone atoms and 1.11 Å for all heavy atoms. Outside of this region, from residue H16 to the N-terminus and from residue F86 to the C-terminus, there is a gradually increasing level of disorder (Figure 2B). The backbone superimposition of the final 20 structures is shown in Figure 3A; toward the end of $\beta$5, the structure was less rigid, which is evident in Figure 2.

*Structure Description.* The tertiary structure of SUMO-3 C47S consists of two α-helices and a mixed $\beta$-sheet. The $\beta$-sheet is composed of three antiparallel $\beta$-strands and one parallel $\beta$-strand (Figure 3B). Overall, the fold of SUMO-3 C47S is highly similar to those of ubiquitin and SUMO-1; helix α1 (residues 39−50) is rotated approximately 45° relative to the first two $\beta$-strands ($\beta$1 and $\beta$2), and this arrangement represents the typical ubiquitin-like conformation. Like SUMO-1, helix α1 is strongly amphipathic in nature, with hydrophobic residues pointing inward and hydrophilic residues pointing into the solvent. Relevant contacts at the helix−sheet interface in SUMO-3 C4S occur between hydrophobic side chains of L19, V21, V29, F31, F59, and I83 of the $\beta$-strands and L39, L42, Y46, and Q50 of helix α1. Sequence alignment of SUMO-3 C47S with its family members and ubiquitin shows that, excluding Q50, these hydrophobic residues are highly conserved (Figure 4A) and appear to be essential for formation of the hydrophobic core. They, together with other conservative residues, I17, I33, F61, I66, L75, and V85, contribute to the maintenance of the ubiquitin fold of SUMO-3 C47S. Helix α2 of SUMO-3 C47S consists of approximately five residues. Long-range NOEs were observed from the N-terminal residues P38 and L39 of helix α1 to residue Q74 of helix α2 and the preceding residues, D70 and T71, making both helices into a conformation perpendicular to each other, which is also a typical ubiquitin fold. Taken together, the structure of SUMO-3 C47S is globular and very compact, except for the last six residues at the carboxyl terminus, which extend away from the core structure and are thus easily accessible to enzymes and substrates.

It has been known that, to produce mature SUMO-3 (residues 1−92), 11 amino acid residues at the C-terminus of the SUMO-3 precursor were removed by the SUMO-specific protease, suggesting that the C-terminal region (residues 93−103) is not essential for the cellular function

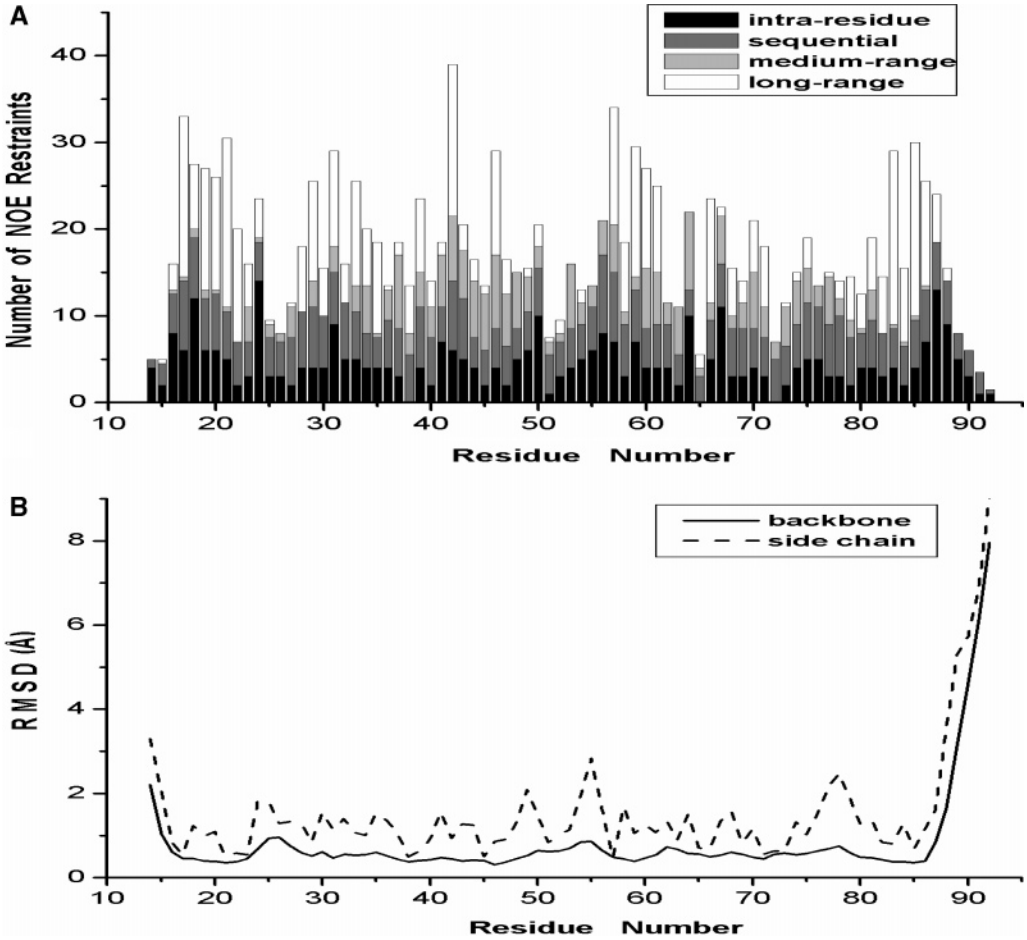


FIGURE 2: (A) Number of NOE restraints per residue used in the calculation of the SUMO-3 C47S structure. (B) Plots of backbone atom and all heavy atom average rmsd values for each residue for the family of 20 structures relative to the mean structure.

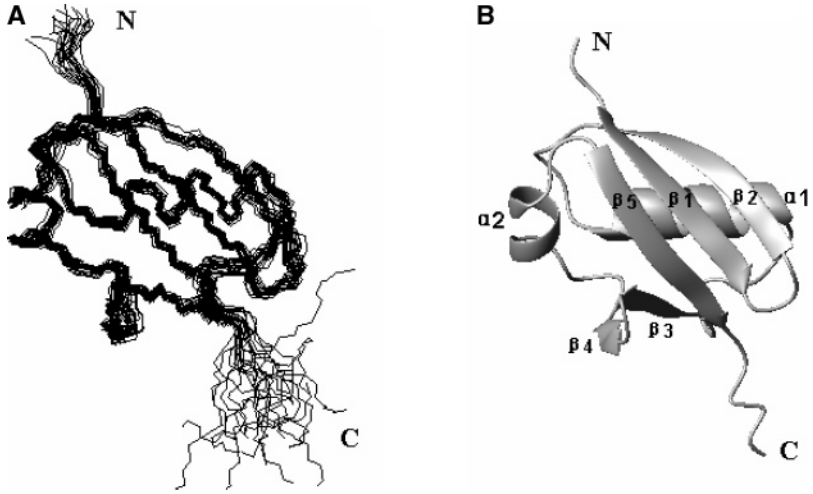


FIGURE 3: NMR structure of SUMO-3 C47S. (A) Backbone superposition of 20 selected conformers from the final CNS calculation. (B) Ribbon representation of the minimized average structure with the secondary structure elements highlighted. This figure was produced with MOLMOL (*38*).

of SUMO-3. A more reasonable explanation might be that the C-terminus, cooperatively with its preceding sequences, provides a bracket for protease to bind and cut. Data from yeast have revealed that the flexible N-terminal extension of SUMO can be entirely deleted and the ubiquitin-like domain is sufficient for conjugation to many substrates and for any downstream interactions required for yeast viability (*37*). There is also evidence that the 21 N-terminal amino acid residues of SUMO-1 are not involved in interaction with E2 enzyme (*17*). The structural integrity of the mutant protein was evaluated by $^1$H NMR spectra. A high degree of similarity was found between the $^1$H NMR spectra of the native SUMO-3 and its mutant. This indicates that the C47S amino acid substitution does not alter the 3D structure of SUMO-3, so this truncated protein with the C47S mutation can be used to substitute SUMO-3 and elucidate the interaction of SUMO-3 with its enzymes. Moreover, because the sequence of SUMO-3 C47S is highly identical (>85%)

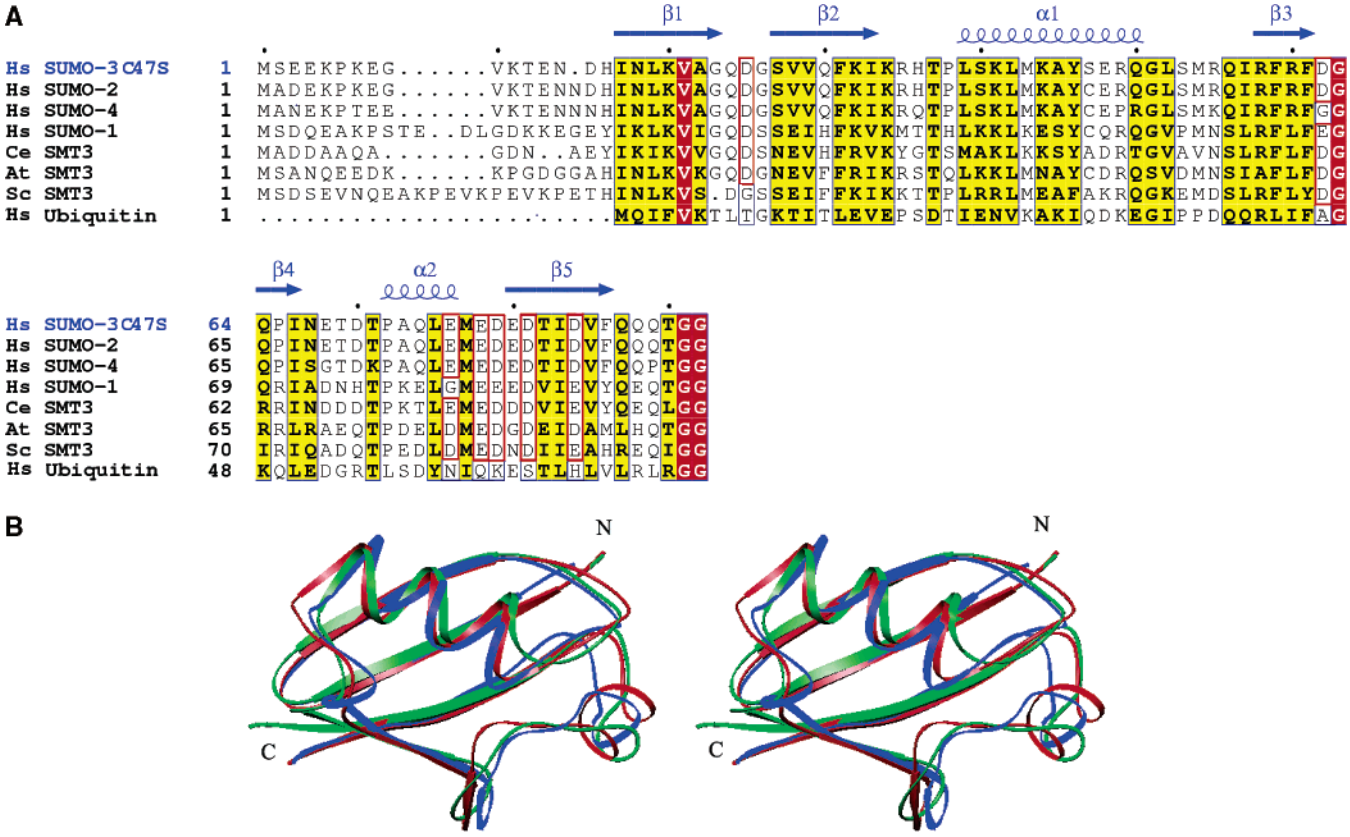


FIGURE 4: (A) Sequence alignment of SUMO-3 C47S with its homologues and ubiquitin: SUMO-3 C47S, SUMO-2, -4, and -1 from *Homo sapiens*, Ce smt3 from *Caenorhabditis elegans*, At smt3 from *Arabidopsis thaliana*, Sc smt3 from *Saccharomyces cerevisiae*, and ubiquitin from *H. sapiens*. The secondary structure of human SUMO-3 C47S is indicated above the alignment. Residues identical in all eight sequences are shown in red columns, and conserved residues are shown in yellow columns. Negative residues conserved in SUMOs, but not in ubiquitin, are boxed in red. The sequence alignment was made using ClustalW. This panel was generated with ESPript 2.2 (*40*). (B) Backbone superposition of the core structures of SUMO-3 C47S (red), SUMO-1 (green), and ubiquitin (blue). Panel B was generated with Ribbons (*41*).

with those of SUMO-2 and -4, this structure can also represent the solution structure of SUMO-2 and -4.

*Structure Comparison with SUMO-1 and Ubiquitin.* It is interesting to find that SUMO-3 C47S overall is more structurally similar to ubiquitin than SUMO-1. The backbone rmsd values between the average minimized structure of SUMO-3 C47S and the structure of SUMO-1 (PDB entry 1A5R) as well as that of ubiquitin (PDB entry 1D3Z) were calculated with the combinatorial extension (CE) method (*39*). SUMO-3 C47S is 46% identical in sequence with SUMO-1 and 14% identical in sequence with ubiquitin; on the other hand, the backbone rmsd value for the core structure of SUMO-3 C47S (residues 16−88) and ubiquitin (residues 1−72) is only 1.4 Å, but the rmsd value for the two core structures of SUMO-3 C47S and SUMO-1 (residues 21−93) is 2.2 Å (Figure 4B).

To further understand the reason, we have calculated the Cα rmsd values for each residue when the core secondary structures of SUMO-3 C47S and SUMO-1 are aligned. Five regions, including two coils (residues 51−57 and 68−71), a turn (residues 61−64), helix α2 (residues 72−75), and the C-terminus of strand $\beta$5 (residues 87 and 88), of SUMO-3 C47S show a greater deviation (>2.0 Å) from the corresponding regions of SUMO-1 (Figure 5A), and coincidently, many residues here are not conserved (Figure 4A). A likely reason is that these regions, extending away from the hydrophobic core, are exposed to solvents. In contrast with SUMO-1, when the core secondary structure of SUMO-3

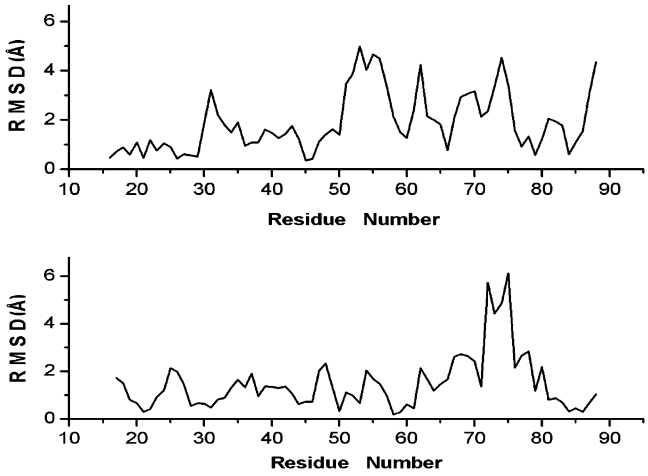


FIGURE 5: Plots of backbone Cα rmsd values for each residue when the core secondary structures are aligned (A) between NMR structures of SUMO-3 C47S and SUMO-1 and (B) between the NMR structures of SUMO-3 C47S and ubiquitin.

C47S is aligned with the ubiquitin structure, only two regions, i.e., a coil (residues 67−70) and helix α2 (residues 72−78) have rmsd values larger than 2.0 Å (Figure 5B). Although a $3_{10}$-helix (residues 38−40) of ubiqintin is not found in SUMO-3 C47S, the Cα rmsd values here are less than 2.0 Å. Collectively, the core structure of SUMO-3 C47S is superimposed well on that of ubiquitin and the overall structure of Ubls is highly conserved.

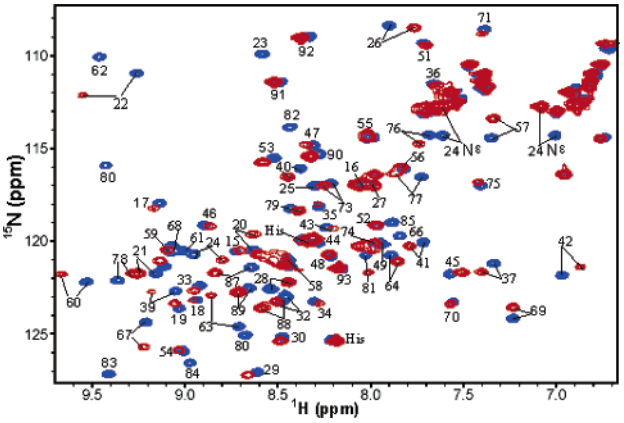


FIGURE 6: Superposition of $^{1}$H−$^{15}$N HSQC spectra of $^{15}$N-labeled human SUMO-3 C47S, free and in complex with Ubc9. The SUMO-3 C47S/Ubc9 ratio is approximately 1:1. The cross-peaks of free SUMO-3 C47S are shown in blue, and those of SUMO-3 C47S in complex are shown in red. All backbone NH and side chain peaks affected by the complex formation are labeled.

*Chemical Shift Perturbation upon Ubc9 Binding.* Specific chemical shift perturbations and changes in the line widths were observed in the $^{1}$H−$^{15}$N HSQC spectrum of SUMO-3 C47S upon formation of the complex with Ubc9. These changes were observed from the beginning of the titration, when the concentration of SUMO-3 C47S was approximately 0.4 mM and that of Ubc9 was 0.04 mM, until the final concentrations of SUMO-3 C47S and Ubc9 reached approximately 0.3 mM. Superposition of the HSQC spectra of free SUMO-3 C47S and that in complex with Ubc9 is shown in Figure 6. The line widths of residues G23, D25, F59, F61, D62, I66, E80, T82, I83, D84, V85, and F86 became so broad in the complex that their cross-peaks cannot be observed from the beginning of the titration when the SUMO-3 C47S/Ubc9 ratio is 10. These residues are likely in intermediate exchange and colored blue in the ribbon diagram of the SUMO-3 C47S structure (Figure 8A).

Residues A22, Q24, I57, R58, G63, N67, M77, and Q87 exhibited combined chemical shift changes of more than the mean value plus one standard deviation (Figure 7). Most of these residues have large chemical shift changes in both the proton and nitrogen dimensions (Figure 6). The chemical shift changes of these residues are linear with the addition of Ubc9. These residues are colored cyan in Figure 8A. In addition, residues K20, V21, G26, V28, T37, L39, S40, L42, R60, T69, E76, E78, D81, and Q88 have combined chemical shift changes larger than the mean value and are colored gray. The resonance of R49 overlaps with that of Q74; therefore, they cannot be monitored. Moreover, the cross-peaks of both protons of the side chain NH2 atom of Q24 shifted significantly, suggesting the formation of hydrogen bonds with certain residues of Ubc9. The two changes in side chain were not found in the SUMO-1−Ubc9 interaction (*17*).

*Ubc9 Binding Surface on SUMO-3 C47S.* The information from chemical shift perturbation given above was used to map the Ubc-9 binding surface on SUMO-3 C47S. Residues 22−25, 57−67, 77, and 80−87 experience the most significant changes in line widths and chemical shifts upon complex formation with Ubc-9 (Figure 8A). All these regions are clustered together spatially, and thus constitute the surface binding to Ubc9. These residues are located in $\beta$-strands 1 and 3−5, the C-terminus of helix α2, the loop between $\beta$1 and $\beta$2, and the sequence between $\beta$3 and $\beta$4. Fifteen of the perturbed residues are conserved in SUMO family members. Among the surface residues that are affected by complex formation, three negatively charged residues, E78, D81, and D84, are highly conserved, but in ubiquitin, they are substituted with neutral or positively charged residues (Figure 4A). In addition, D25 and D62 are moderately conserved among SUMO family members. These residues and other electronegative residues, E76, D79, and E80, constitute a large negative potential surface (Figure 8B). The observation suggests an important role for electrostatic attractions in the interaction between SUMO-3 C47S and Ubc9. Seven hydrophobic residues, i.e., I57, F59, F61, I66, M77, I83, and V85, on the binding surface are highly conserved throughout different species (Figure 4A). In particular, F61 and M77 are exposed to solvent, which may form hydrophobic interactions with Ubc9. On the contrary, many positively charged residues, including K32, K34, R35, H36, K41, K44, R49, and R55, are located on the other semiglobular surface, which is a distinct positive potential surface (Figure 8C) and does not interact with Ubc9.

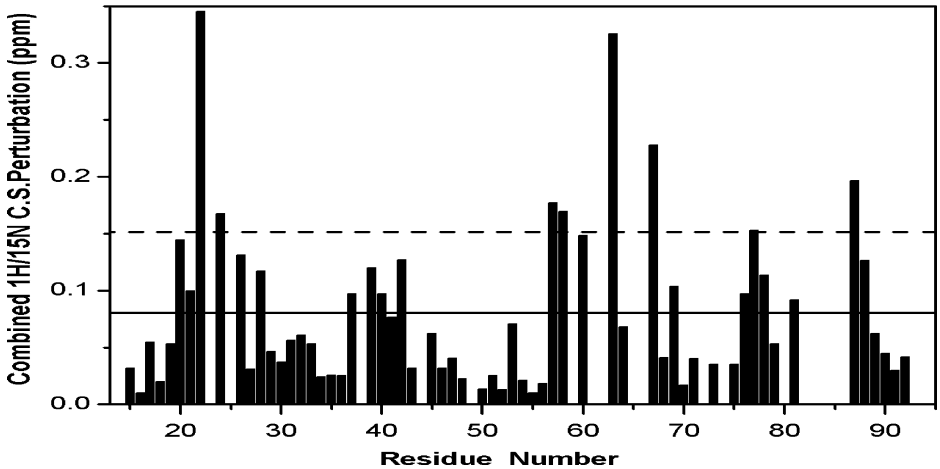


FIGURE 7: Histogram of the chemical shift perturbation of SUMO-3 C47S by addition of Ubc9. The mean value is shown as a solid line and the mean value plus one standard deviation as a dashed line. The combined $^{1}$H and $^{15}$N chemical shift changes are defined as $\Delta\delta_{ppm} = \sqrt{(\Delta\delta_{HN})^2 + (\Delta\delta_N\alpha_N)^2}$, and the scaling factor $\alpha_N$ used to normalize the $^{1}$H and $^{15}$N chemical shift is 0.17. Residues whose cross-peaks are not observed in the presence of Ubc9 are excluded.

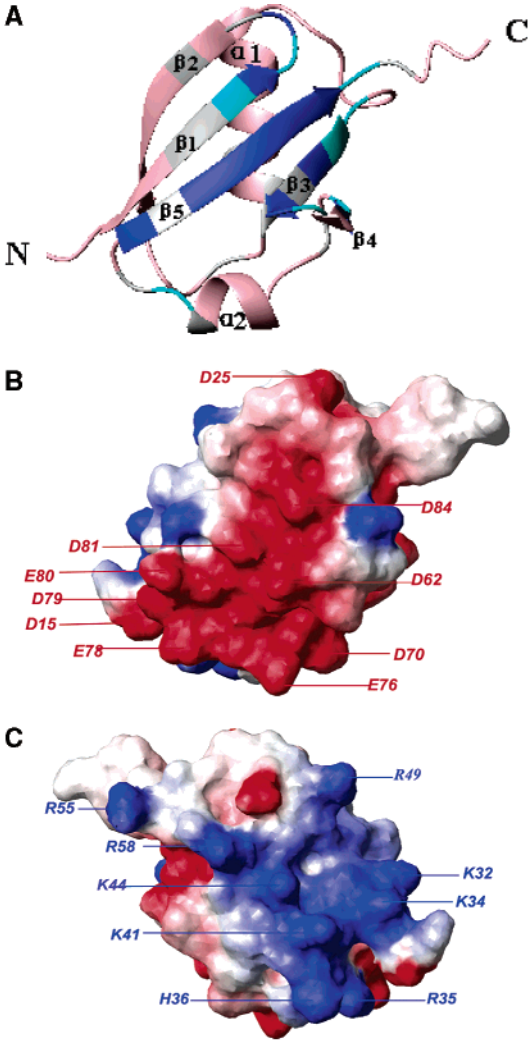


FIGURE 8: (A) Ribbon diagram showing the chemical shift perturbation of SUMO-3 C47S upon binding of Ubc9. Those residues whose cross-peaks disappeared in the titration are colored blue; the residues whose combined chemical shift changes were more than the mean value plus one standard deviation and above the mean value are colored cyan and gray, respectively. (B) Surface electrostatic potential of human SUMO-3 C47S. The orientation of the molecule in panel B is the same as that in panel A. Red corresponds to negative potentials, and the electronegative residues are marked. (C) Surface potential rotated 180° from panel B about a vertical axis in the plane of the paper. Blue corresponds to positive potentials, and the electropositive residues are marked. The charge topology was calculated and displayed using MOLMOL (*38*).

As reported previously, the SUMO-3 binding site on Ubc9 mainly resides on helices α1 and α2, β-strands 1−3, and the loop between α1 and β1 (*42*). These regions that are clustered together in the three-dimensional structure of Ubc9 constitute the surface binding to SUMO-3. Five electropositive residues, i.e., K14, R17, K18, H20, and K110, exhibit significant perturbation upon SUMO-3 binding. These highly conserved residues, together with adjacent R13 and K30, constitute a large positive potential surface as shown in Figure 2B (*17*). This surface is apparently compatible with the negative potential surface of SUMO-3. Consistent with that, R13A/K14A and R17A/K18A mutations in Ubc9 disrupted the interaction with SUMO (*42*). Furthermore, six hydrophobic residues affected significantly are also conserved between the human and yeast proteins. In a word, for SUMO-3 C47S and Ubc9, similar numbers of oppositely charged residues and hydrophobic residues at the binding interfaces are conserved. This suggests the high compatibility of the binding interfaces.

Thus, we can draw a conclusion that the Ubc9 binding surface on SUMO-3 C47S is located on the hydrophilic side of the β-sheet, and complementary surface electrostatic potential plus hydrophobic interactions contributes to the specific binding of SUMO-3 C47S to Ubc9. A previous perturbation study has shown that the Ubc9 binding site on SUMO-1 consists of residues 26, 64−71, and 81−91 (*17*). Like SUMO-3 C47S, this surface bears negative charge, thereby interacting with the positively charged region of Ubc9. As a whole, the binding interface is conserved in SUMO−E2 interactions. In addition, SUMO-3 C47S shows a few specific residues perturbed upon formation of the SUMO-3−Ubc9 complex, which may result from the sequence and structure differences between the two isoforms.

*Mechanism of SUMO Distinguishing Ubc9 from Ubiquitin E2s.* To our knowledge, SUMO has a single E2-type-conjugating enzyme, Ubc9, which is specific for SUMO and does not act on ubiquitin (*43*, *44*). Although the three-dimensional structures are highly conserved between SUMO-3 C47S and ubiquitin, the surface electrostatic potentials between the two proteins are very different. The surface of SUMO-3 C47S that binds Ubc9 has an overall negative electrostatic potential. However, this surface of ubiquitin is positively charged (*13*). A structural comparison of Ubc9 with ubiquitin-specific E2 enzymes (Ubc4 and Ubc7) revealed that, despite an overall similarity, the surface electrostatic potentials were quite different (*45*). The surface of Ubc9, which is involved in SUMO binding, is mainly positively charged, whereas the corresponding regions in ubiquitin-specific E2s have negative or neutral potentials. These differences are likely to have a role in modifier discrimination. Notably, the negatively charged surface of SUMO is highly complementary in its electrostatic potentials to the positively charged surface of Ubc9. On the basis of a similar reason, ubiquitin interacts with Ubc4 and Ubc7 but cannot bind to Ubc9. Despite a surprising similarity in modification mechanism, sumoylation and ubiquitylation have their own enzymes, independent pathway, and distinct functions.

## CONCLUSIONS

We have determined the solution structure of SUMO-3 C47S which is the second NMR structure of human SUMO family members. Comparably, SUMO-3 C47S is more structurally similar with ubiquitin rather than SUMO-1. The hydrophobic residues at the helix−sheet interface are highly conserved, and they contribute to the maintenance of the globular and compact ubiquitin fold. Two glycine residues at the C-terminus that are involved in the formation of an isopeptide bond with a target protein extend away from the core structure. At the same time, we have studied the interaction between SUMO-3 C47S and its E2 enzyme by chemical shift perturbation. Residues 22−25, 57−67, 77, and 80−87 exhibit the most significant changes in line widths and chemical shifts upon formation of the complex with Ubc-9. All these residues are clustered together in the three-dimensional structure of SUMO-3 C47S. Among the SUMO family members, the negatively charged and hydrophobic

residues in the binding surface are highly or moderately conserved. Apparently, complementary surface electrostatic potential and hydrophobic interactions contribute to SUMO-3 C47S-specific binding to Ubc9.

## ACKNOWLEDGMENT

We thank Dr. Ronald T. Hay for providing the full-length human Ubc9 cDNA in pGEX-2T, Dr. F. Delaglio and Prof. A. Bax for providing NMRPipe, Prof. T. D. Goddard and Prof. D. G. Kneller for providing Sparky, Prof. A. T. Brünger for providing CNS, Dr. R. Koradi and Prof. K. Wüthrich for providing MOLMOL, and M. Carson for providing Ribbons.

## REFERENCES

1. Müller, S., Hoege, C., Pyrowolakis, G., and Jentsch, S. (2001) SUMO, ubiquitin's mysterious cousin, *Nat. Rev. Mol. Cell Biol. 2*, 202−210.
2. Gill, G. (2003) Post-translational modification by the small ubiquitin-related modifier SUMO has big effects on transcription factor activity, *Curr. Opin. Genet. Dev. 13*, 108−113.
3. Su, H. L., and Li, S. S.-L. (2002) Molecular features of human ubiquitin-like SUMO genes and their encoded proteins, *Gene 296*, 65−73.
4. Bohren, K. M., Nadkarni, V., Song, J. H., Gabbay, K. H., and Owerbach, D. (2004) A M55V polymorphism in a novel SUMO gene (SUMO-4) differentially activates heat shock transcription factors and is associated with susceptibility to type I dibetes mellitus, *J. Biol. Chem. 279*, 27233−27238.
5. Seeler, J. S., and Dejean, A. (2003) Nuclear and unclear functions of SUMO, *Nat. Rev. Mol. Cell Biol. 4*, 690−699.
6. Rodriguez, M. S., Dargemont, C., and Hay, R. T. (2001) SUMO-1 conjugation *in vivo* requires both a consensus modification motif and nuclear targeting, *J. Biol. Chem. 276*, 12654−12659.
7. Li, S. J., and Hochstrasser, M. (1999) A new protease required for cell-cycle progression in yeast, *Nature 398*, 246−251.
8. Saitoh, H., and Hinchey, J. (2000) Functional heterogeneity of small ubiquitin-related protein modifiers SUMO-1 versus SUMO-2/3, *J. Biol. Chem. 275*, 6252−6258.
9. Azuma, Y., Arnaoutov, A., and Dasso, M. (2003) SUMO-2/3 regulates topoisomerase II in mitosis, *J. Cell Biol. 163*, 477−487.
10. Zhao, Y., Kwon, S. W., Anselmo, A., Kaur, K., and White, M. A. (2004) Broad-spectrum identification of cellular SUMO substrate proteins, *J. Biol. Chem. 279*, 20999−21002.
11. Tatham, M. H., Jaffray, E., Vaughan, O. A., Desterro, J. M., Botting, C. H., Naismith, J. H., and Hay, R. T. (2001) Polymeric chains of SUMO-2 and SUMO-3 are conjugated to protein substrates by SAE1/SAE2 and Ubc9, *J. Biol. Chem. 276*, 35368−35374.
12. Tong, H., Hateboer, G., Perrakis, A., Bernards, R., and Sixma, T. K. (1997) Crystal structure of murine/human Ubc9 provides insight into the variability of the ubiquitin-conjugating system, *J. Biol. Chem. 272*, 21381−21387.
13. Bayer, P., Arndt, A., Metzger, S., Mahajan, R., Melchior, F., Jaemicke, R., and Becker, J. (1998) Structure determination of the small ubiquitin-related modifier SUMO-1, *J. Mol. Biol. 280*, 275−286.
14. Jin, C., Shiyanova, T., Shen, Z., and Liao, X. (2001) Heteronuclear nuclear magnetic resonance assignments, structure and dynamics of SUMO-1, a human ubiquitin-like protein, *Int. J. Biol. Macromol. 28*, 227−234.
15. Vijay-Kumar, S., Bugg, C. E., and Cook, W. J. (1987) Structure of ubiquitin refined at 1.8 Å resolution, *J. Mol. Biol. 194*, 531−544.
16. Cornilescu, G., Marquardt, J. L., Ottiger, M., and Bax, A. (1998) Validation of protein structure from anisotropic carbonyl chemical shifts in a dilute liquid crystalline phase, *J. Am. Chem. Soc. 120*, 6836−6837.
17. Liu, Q., Jin, C., Liao, X., Shen, Z., Chen, D., and Chen, Y. (1999) The binding interface between an E2 (UBC9) and a ubiquitin homologue (UBL1), *J. Biol. Chem. 274*, 16979−16987.
18. Sheng, W., and Liao, X. (2002) Solution structure of a yeast ubiquitin-like protein Smt3: The role of structurally less defined sequences in protein−protein recognitions, *Protein Sci. 11*, 1482−1491.
19. Mossessova, E., and Lima, C. D. (2000) Ulp1-SUMO crystal structure and genetic analysis reveal conserved interactions and a regulatory element essential for cell growth in yeast, *Mol. Cell 5*, 865−876.
20. Bax, A., Ikura, M., Kay, L. E., Torchia, D. A., and Tschudin, R. (1990) Comparison of different modes of two-dimensional reverse correlation NMR for the study of proteins, *J. Magn. Reson. 86*, 304−318.
21. Muhandiram, D. R., and Kay, L. E. (1994) Gradient-enhanced triple resonance three-dimensional NMR experiments with improved sensitivity, *J. Magn. Reson., Ser. B 103*, 203−216.
22. Clubb, R. T., Thanabal, V., and Wagner, G. (1992) A constant-time 3-dimensional triple-resonance pulse scheme to correlate intraresidue H-1(N), N-15, and C-13 chemical shifts in N-15-C-13-labeled proteins, *J. Magn. Reson. 97*, 213−217.
23. Grzesiek, S., and Bax, A. (1992) Correlating backbone amide and side chain resonances in larger proteins by multiple relayed triple resonance NMR, *J. Am. Chem. Soc. 114*, 6291−6293.
24. Grzesiek, S., and Bax, A. (1992) An efficient experiment for sequential backbone assignment of medium-sized isotopically enriched proteins, *J. Magn. Reson. 99*, 201−207.
25. Logan, T. M., Olejniczak, E. T., Xu, R. X., and Fesik, S. W. (1993) A general method for assigning NMR spectra of denatured proteins using 3D HC(CO)NH-TOCSY triple resonance experiments, *J. Biomol. NMR 3*, 225−231.
26. Bax, A., Clore, G. M., and Gronenborn, A. M. (1990) $^{1}H-^{1}H$ correlation via isotropic mixing of $^{13}C$ magnetization, a new three-dimensional approach for assigning $^{1}H$ and $^{13}C$ spectra of $^{13}C$-enriched proteins, *J. Magn. Reson. 88*, 425−431.
27. Bax, A., Clore, G. M., Driscoll, P. C., Gronenborn, A. M., Ikura, M., and Kay, L. E. (1990) Practical aspects of proton-carbon−carbon-proton three-dimensional correlation spectroscopy of $^{13}C$-labeled proteins, *J. Magn. Reson. 87*, 620−627.
28. Grzesiek, S., and Bax, A. (1993) Amino acid type determination in the sequential assignment procedure of uniformly $^{13}C/^{15}N$-enriched proteins, *J. Biomol. NMR 3*, 185−204.
29. Yamazaki, T., Formankay, J. D., and Kay, L. E. (1993) Two-Dimensional NMR experiments for correlating C-13-$\beta$ and H-1-$\delta/\epsilon$ chemical-shifts of aromatic residues in C-13-labeled proteins via scalar couplings, *J. Am. Chem. Soc. 115*, 11054−11055.
30. Zuiderweg, E. R. P., and Fesik, S. W. (1989) Heteronuclear three-dimensional NMR spectroscopy of the inflammatory protein C5a, *Biochemistry 28*, 2387−2391.
31. Barkhuijsen, H., de Beer, R., Bovee, W. M., Creyghton, J. H., and van Ormondt, D. (1985) Application of linear prediction and singular value decomposition (LPSVD) to determine NMR frequencies and intensities from the FID, *Magn. Reson. Med. 2*, 86−89.
32. Nilges, M. (1993) A calculation strategy for the structure determination of symmetric dimers by $^{1}H$ NMR, *Proteins 17*, 297−309.
33. Wishart, D. S., and Sykes, B. D. (1994) The $^{13}C$ chemical-shift index: A simple method for the identification of protein secondary structure using $^{13}C$ chemical-shift data, *J. Biomol. NMR 4*, 171−180.
34. Brunger, A. T., Adams, P. D., Clore, G. M., Delano, W. L., Gros, P., Grosse-Kunstleve, R. W., Jiang, J.-S., Kuszewski, J., Nilges, M., Pannu, N. S., Read, R. J., Rice, L. M., Simonson, T., and Warren, G. L. (1998) Crystallography & NMR system: Anew software suite for macromolecular structure determination, *Acta Crystallogr. D54*, 905−921.
35. Stein, E. G., Rice, L. M., and Brunger, A. T. (1997) Torsion-angle molecular dynamics as a new efficient tool for NMR, *J. Magn. Reson. 124*, 154−164.
36. Laskowski, R. A., Rullmann, J. A., MacArthur, M. W., Kaptein, R., and Thornton, J. M. (1996) AQUA and PROCHECK-NMR: Programs for checking the quality of protein structure solved by NMR, *J. Biomol. NMR 8*, 477−486.
37. Bylebyl, G. R., Belichenko, I., and Johnson, E. S. (2003) The SUMO isopeptidase Ulp2 prevents accumulation of SUMO chains in yeast, *J. Biol. Chem. 278*, 44113−44120.
38. Koradi, R., Billeter, M., and Wüthrich, K. (1996) MOLMOL: A program for display and analysis of macromolecular structures, *J. Mol. Graphics 14*, 51−55.

39. Shindyalov, I. N., and Bourne, P. E. (1998) Protein structure alignment by incremental combinatorial extension (CE) of the optimal path, *Protein Eng. 11*, 739−747.
40. Gouet, P., Courcelle, E., Stuart, D. I., and Metoz, F. (1999) ESPript: Analysis of multiple sequence alignment in PostScript, *Bioinformatics 15*, 305−308.
41. Carson, M. (1987) Ribbon models of macromolecules, *J. Mol. Graphics 5*, 103−106.
42. Tatham, M. H., Kim, S., Yu, B., Jaffray, E., Song, J., Zheng, J., Rodriguez, M. S., Hay, R. T., and Chen, Y. (2003) Role of an N-terminal site of Ubc9 in SUMO-1, -2, and -3 conjugation, *Biochemistry 42*, 9959−9969.
43. Desterro, J. M., Thomson, J., and Hay, R. T. (1997) Ubch9 conjugates SUMO but not ubiquitin, *FEBS Lett. 417*, 297−300.
44. Schwarz, S. E., Matuschewski, K., Liakopoulos, D., Scheffner, M., and Jentsch, S. (1998) The ubiquitin-like proteins SMT3 and SUMO-1 are conjugated by the UBC9 E2 enzyme, *Proc. Natl. Acad. Sci. U.S.A. 95*, 560−564.
45. Giraud, M. F., Desterro, J. M., and Naismith, J. H. (1998) Structure of ubiquitin-conjugating enzyme 9 displays significant differences with other ubiquitin-conjugating enzymes which may reflect its specificity for sumo rather than ubiquitin, *Acta Crystallogr. D54*, 891−898.

BI0477586